Available online at www.sciencedirect.com

ScienceDirect

Advances in Space Research 66 (2020) 1551–1557

ADVANCES IN SPACE RESEARCH (a COSPAR publication)

www.elsevier.com/locate/asr

Experimental studies of Ka Band Rain Fade Slope at a Tropical Location of India

Saurabh Das [a,*], Madhura Chakraborty [b], Swastika Chakraborty [c], Ashish Shukla [d], Rajat Acharya [d]

[a] Discipline of Astronomy, Astrophysics and Space Engineering, Indian Institute of Technology Indore, India
[b] JIS College of Engineering, Kalyani, Nadia, India
[c] Sikkim Manipal Institute of Technology, Sikkim Manipal University, Rangpo, India
[d] Space Applications Centre, ISRO, Ahmedabad, India

Received 1 November 2019; received in revised form 26 May 2020; accepted 11 June 2020
Available online 26 June 2020

Abstract

Dynamic characteristics of Ka band rain fade (or rain attenuation) over tropical region are relatively less studied, though they are essential for implementation of suitable fade mitigation techniques. In this paper, dynamic characteristics of rain fade at 20 GHz and 30 GHz from GSAT-14 satellite are reported with experimental measurements at Ahmedabad, India. ITU-R model for fade slope probability distribution has been analyzed in this paper and Ka band rain fade has been investigated based on this fade-slope analysis. The ITU-R model is found to closely match 20 GHz measurements, though differences increase at 30 GHz. Fade slopes are found to be within ±0.5 dB/s at both 20 and 30 GHz. Both positive and negative slopes of the fade slope distributions are quasi-similar. ITU-R model's *s* parameter, relating fade slope to filter characteristics, is found to be very close to the measured value for this region. Distributions of fade slopes are also found to be dependent on the standard deviation values similar to ITU-R recommendation at 20 GHz, but significant deviation is observed at 30 GHz. This observed frequency dependency might be due to increase in cloud attenuation at high frequencies or may be due to limited data set. Results indicate needs of further experimental data at high frequencies from other tropical regions to gain further insight into the fade slope characteristics. This will ultimately help in designing a better prediction model in future.

Keywords: Fade slope; Ka band beacon measurements; Satellite communication; Tropical region; *s* parameter

1. Introduction

Knowledge on dynamic rain fade or rain attenuation characteristics is required for designing adaptive fade countermeasure of a satellite communication link operating above 10 GHz frequency (Castanet et al., 2003). As more communication designs exploit Ka/V band, rain attenuation has become a challenging issue. The conventional uplink power control (ULPC) is insufficient to mitigate such a high amount of attenuation during rainy period. Over tropical and equatorial regions, this becomes more serious due to frequent occurrences of heavy convective type of rain (Das et al., 2010, 2013), which usually leads to a very high rain fade for a significant time of a year. High link availability demands implementations of proper adaptive fade counter measures (Castanet et al., 2003; Sarkar et al., 2014; Ventouras et al., 2001), which in turn, depend on both first and second order characteristics of rain attenuation, i.e. both fade amount and fade slope (Cheffena & Amaya, 2008; Kamp, 2003).

* Corresponding author.
E-mail addresses: das.saurabh01@gmail.com, saurabh.das@iiti.ac.in (S. Das).

https://doi.org/10.1016/j.asr.2020.06.014
0273-1177/

Several studies on prediction of rain attenuation and characteristics of fade slope at high frequencies were carried out over temperate locations (Kamp, 2003; Amaya & Nguyen, 2010; Xin et al., 2012; Green, 2004). However, such information on tropical or equatorial regions is limited and most of it is focused only on the 1st order characteristics of rain attenuation (Green, 2004). The 2nd order rain fade characteristic such as fade slope is also an important parameter in designing of efficient fade mitigation techniques. As rain characteristics change significantly over tropical regions, commonly used ITU-R models are found inadequate for prediction of rain attenuation and also in the modeling of related propagation impairments (Adhikari et al., 2011; Sujimol et al., 2015; Pontes et al., 2003; Miranda et al., 1999, Debnath et al., 2017; Ong et al., 1997). Therefore, experimental studies of fade slope characteristics at different frequencies over tropical regions are essential (Das & Maitra, 2016; Jong et al., 2019). In this paper, we present the experimental characteristics of fade slope observed in Ahmedabad (23°04′, 73°38′), a tropical Indian location, where 20/30 GHz signals are measured from GSAT-14 satellite and thereby a detailed analysis of the existing ITU-R (ITU-R P.1623 –1, 2005) fade slope distribution model has been done for this tropical location in Ka band.

2. Methodology

2.1. Experimental description

Ka band signal from GSAT-14 satellite has been recorded at Space Applications Centre, ISRO, Ahmedabad during 2014 to 2016 with a 2.4 m antenna at an elevation angle of 63°. The GSAT-14 is located at the Geostationary orbit at 74°E and transmits linearly polarized signals with an EIRP of 24 dBw. This experiment is a part of "Ka band propagation experiment" in collaboration with CNES/ONERA. The horizontally polarized beacon signal is measured with a Ka band receiver with 1 Hz sampling rate at 20.2 and 30.5 GHz (here after, just mentioned as 20 and 30 GHz). The 20 GHz data has been obtained for 3 years (2014–2016; except August 2015, October 2015 and December 2015 to February 2016) while only 10 months of data is available for 30 GHz (June 2014 to March 2015) due to instrument irregularity. The data set for every month is almost continuous with occasional (as already mentioned) data gap. For 20 GHz, the data availability was almost 86% and for 30 GHz it was 83% of the total measurement time. The rain is also measured for the same period with a tipping bucket rain gauge and an impact type disdrometer. The rain rate (mm/hr) is measured with 30 s temporal resolution.

Ahmedabad is located in a hot, semi arid climate with extremely dry weather throughout the year except during the monsoon (June-Sept). The typical average annual rainfall is around 80 cm that occurs mostly during the monsoon. The rain is characterized by frequent heavy rainfall during this period. Both convective rain and stratiform rain occur at this place, but majority of the rain is of stratiform type (Das & Maitra, 2017).

2.2. Data pre-processing

The analog signal is received in volts, which get digitized by Analog to Digital Converter (ADC), and after due signal processing, the signal is converted into dB. In case of Ka band beacon receiver, the measurement is converted in dB value by taking into account signal level corresponding to clear sky signal level at low noise amplifier (LNA) input of the receiver. Clear sky signal level is considered taking into account Effective isotropic radiated power (EIRP), Path loss (satellite to receiver path), Cable loss (spectrum analyzer to low noise amplifier), Antenna Gain and Low noise amplifier Gain. Calibration curve is taken as the plot of signal level corresponding to clear sky signal level at low noise amplifier (LNA) input of receiver in dB versus voltage. The measurements have an accuracy level of ±0.5 dB.

A 10th order low-pass Butterworth filter of 0.025 Hz cut off frequency then filters out the scintillation. The cutoff frequency is based on the power spectral analysis of the received signal as shown in Fig. 1. The slope of the power spectral density of rain attenuation is different from that of scintillation (Matricciani & Riva, 2008). The cut off frequency is chosen at the point where the slope of the power spectral density of the signal changes.

At the time of calculation, rainy and non-rainy days are first segregated. As a clear variation of signal level for each month is observed, first the non-rainy days, approximately 11–12 days per month during monsoon, are separated. This process is repeated for each year for 20 GHz data and only for the year 2014 for 30 GHz data. The signal level values of these non-rainy days in each month are then separately averaged before being filtered. Average non-rainy clear sky signal level is further processed by filtering with same cut off frequency for removing scintillation. This clear sky level

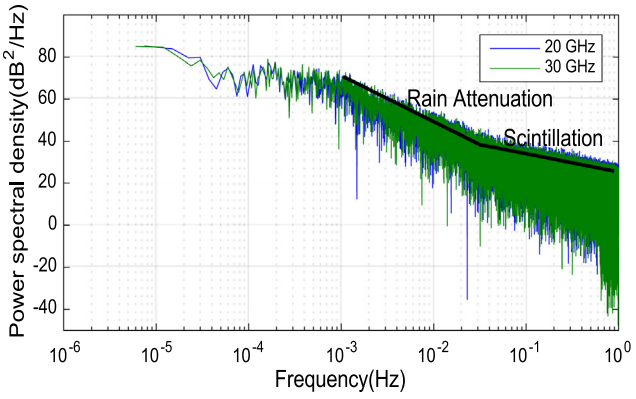

Fig. 1. Power Spectral Density of the rain attenuation and scintillation (Year 2014 for both the frequency).

is later used as reference signal level for finding attenuation (dB) for that particular month. The total attenuation is calculated by subtracting reference signal level (dB) from the measured signal level (dB) during rain. The total attenuation has been considered here as no separation of rain attenuation has been done from cloud attenuation. However, the gaseous attenuation has been removed from time series in this process. As attenuation due to rain is much higher at the considered frequency band than the attenuation due to the rest of the atmospheric constituents, here it has been mentioned simply as rain attenuation.

The measured rain attenuation is later used for further processing. In this work, 1 sec temporal resolution data have been used and the equation to estimate the fade slope is:

$$\zeta(\mathrm{i}) = \frac{A(i+1) - A(i-1)}{2}(\mathrm{dB/s}) \quad (1)$$

where A is the attenuation value, i is the i^{th} time instant, ζ is the slope.

Here the time interval is taken as 2 sec for calculating fade slope.

3. Results

3.1. Specific rain attenuation

Fig. 2 shows an instance of severe decrease of signal strength during rain as observed in Ahmedabad on 17 July, 2014. The corresponding rain rate and rain drop size distribution are shown in the same figure. Large drops are evident during heavy rain and associated decrease in signal strength is also very large. In fact, the drop in signal strength was more than 30 dB and signal was lost for a significant time for rain rates >60 mm/hr at both the frequencies.

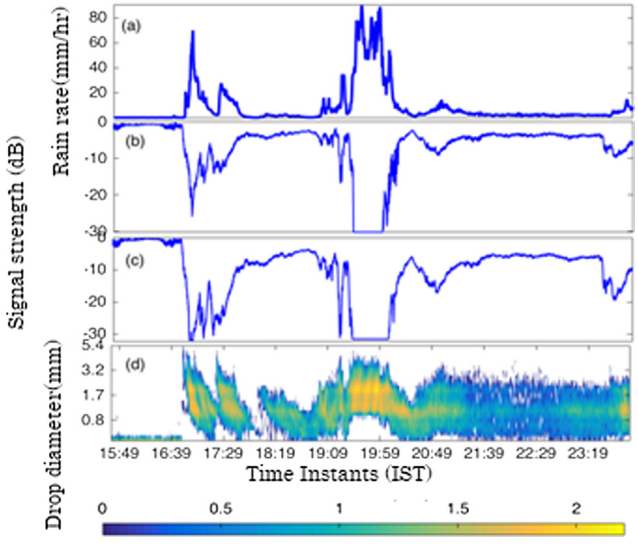

Fig. 2. An example of the rain attenuation over Ahmedabad (event date:17th July 2014). (a) rain rate(mm/hr), (b) signal strength (dB) at 20 GHz, (c) signal strength (dB) at 30 GHz, and (d) corresponding DSD (m^{-3} mm^{-1}). The DSD concentration is in log base 10 scale in colour bar.

The specific rain attenuation (γ) is usually modeled in terms of rain rate (R) as $\gamma = kR^{\alpha}$ where k and α are obtained from experimental measurements. For this purpose, the received signal and rain rate are first time synchronized. Here, the rain rate data has been collected using a disdrometer. Received rain attenuation is then converted to specific attenuation using the calculated path length as per ITU-R (ITU-R P.618-13, 2017) following which the rain rate and specific attenuation are simultaneously plotted. Next, the power law coefficient, k and α, are estimated by power law function using MATLAB software. Here, only the data of 2014 is considered for both the frequencies. Table 1 describes both measured and ITU-R recommended coefficient values for both the frequencies. It is observed that the ITU-R recommended coefficient values are slightly different from the measured values (for both k and α) of both the frequencies. This slight difference may be due to the use of instantaneous DSD measurements in comparison to the global average DSD used in ITU-R (ITU-R P.838–3) for calculation of k and α.

3.2. Fade slope characteristics

Fig. 3 indicates the number of data points exceeding the mentioned attenuation threshold. Since in our case, the time resolution is 1 s, the numbers of data points essentially indicate the total time exceeded by such attenuation threshold. The slope of the curve changes after 7 dB in case of 20 GHz data, thereby indicating a change in the type of rain. High fades are usually associated with convective events, which are less probable than low rain rate stratiform events. However, from the figure one can note that high fades are encountered in Ahmedabad for a significant percentage of time, which is a general characteristic of tropical regions (Das & Maitra, 2017).

The conditional probability densities of rain fade slopes for different threshold attenuation values for both the frequencies are shown in Fig. 4. Bin size is taken as 0.001 dB/s for ζ and 1 dB for A. The fade slopes are symmetrically distributed around 0 dB/s, for both the frequencies, with a spread that increases with increase in attenuation. The maximum fade slope is found to be within ±0.5 dB/s for both the frequencies. ITU-R model predicted

Table 1
Coefficient values for Ahmedabad for the Year 2014 (20 GHz and 30 GHz).

Model	Frequency	k	α
ITU-R	20 GHz	0.09164	1.0568
Measured		0.1017	1.142
ITU-R	30 GHz	0.2923	0.9676
Measured		0.2403	0.9485

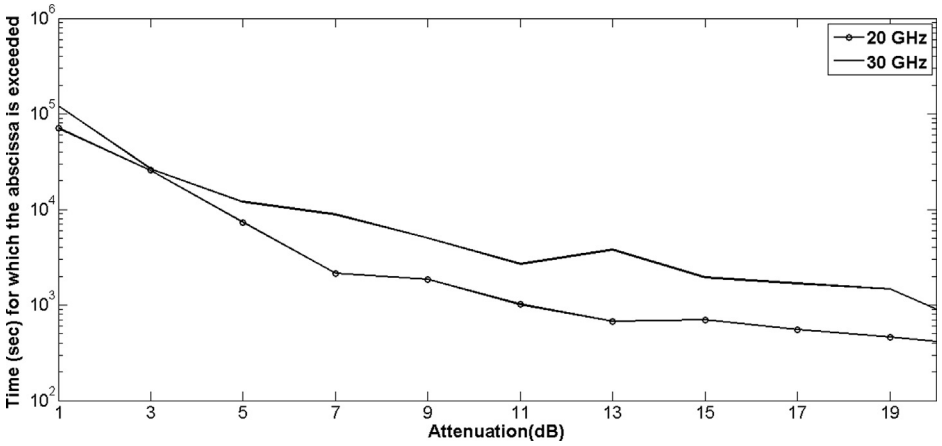

Fig. 3. Time (sec) for which the attenuation threshold in abscissa is exceeded in 2014.

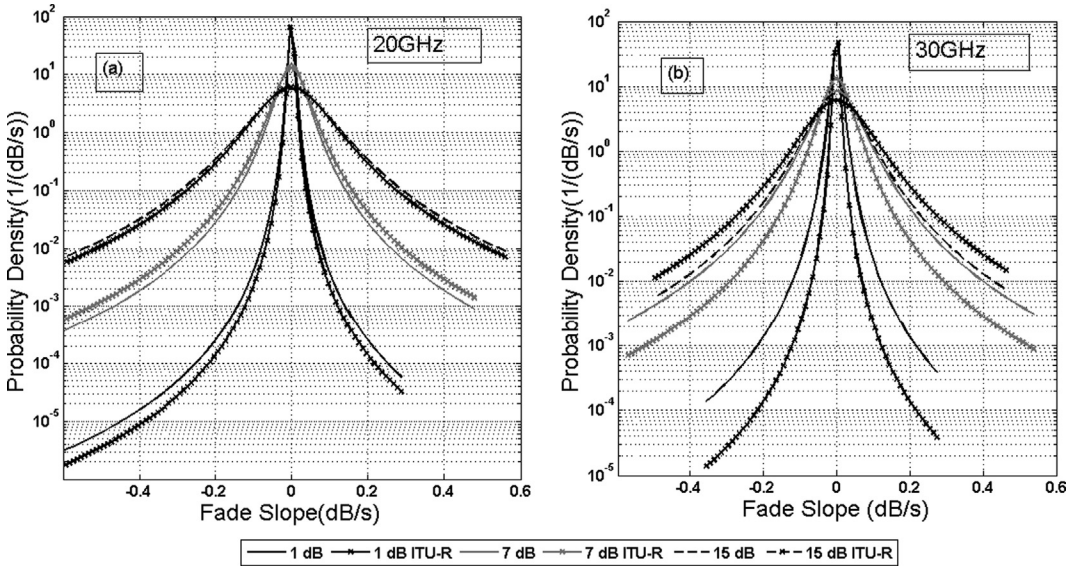

Fig. 4. Modeled conditional distribution of fade slope with ITU-R model at (a) 20 GHz and (b) 30 GHz.

distributions are shown in the same figure by star marked lines. Though the ITU-R model closely matches the 20 GHz frequency data, it shows significant variations from the experimental data at 30 GHz. ITU-R model assumes that the distribution is dependent only on the standard deviation values and is independent of frequency. But, the observed discrepancy between measured and ITU-R model indicates a frequency dependency. Similar observations are also reported from a few other locations such as Delhi (Sujimol et al., 2015), Malaysia (Dao et al., 2013, 2018) and Southern England (Chambers et al., 2006). However, it should be emphasized here that more data from other locations and further investigations are essential to conclude this point.

In order to investigate it further, standard deviations are plotted against the attenuation threshold values in Figs. 5 and 6. It can be seen that the standard deviations of fade slopes are increasing in nature for both the frequencies and are similar to ITU-R model based standard deviation variation. However, it deviated from the experimental standard deviation curve after a certain attenuation threshold value. For better understanding, the numbers of data points considered for calculating the fade slope standard deviation, for both the frequencies, are also plotted on the same figure. At 20 GHz, the total span of measurement covers three consecutive years (2014–2016) whereas the data availability for 30 GHz is limited to a span of one-year (only 2014). From Fig. 5, good agreement between model and measured standard deviation for 20 GHz is observed upto 12 dB and the discrepancy starts beyond that point. From the observed number of data points, it can be concluded that at 20 GHz, beyond 12 dB attenuation, the standard deviation of fade slope may not be statistically very stable. On the other hand, as per Fig. 6,

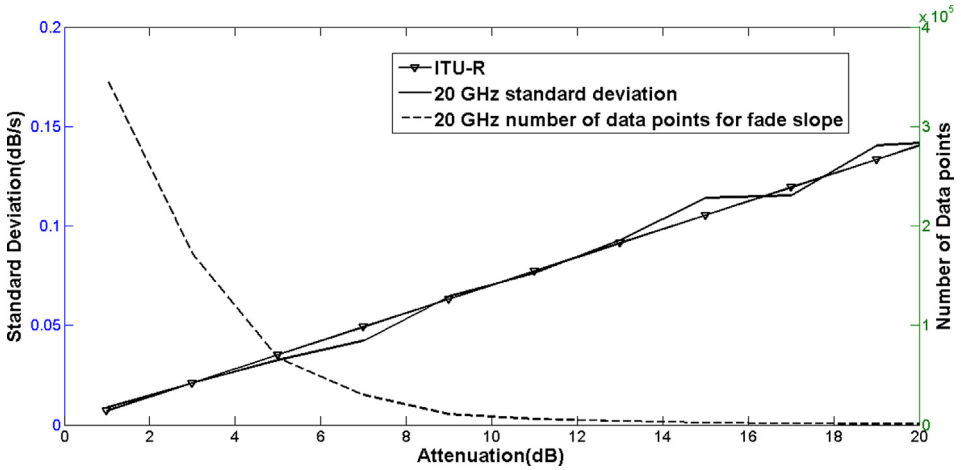

Fig. 5. Fade slope standard deviation as a function of attenuation, at 20 GHz in the period 2014–2016 (solid line), compared to the ITU-R model predictions (solid line with triangle) and number of data points considered for calculation of fade slope (dashed line) for 20 GHz.

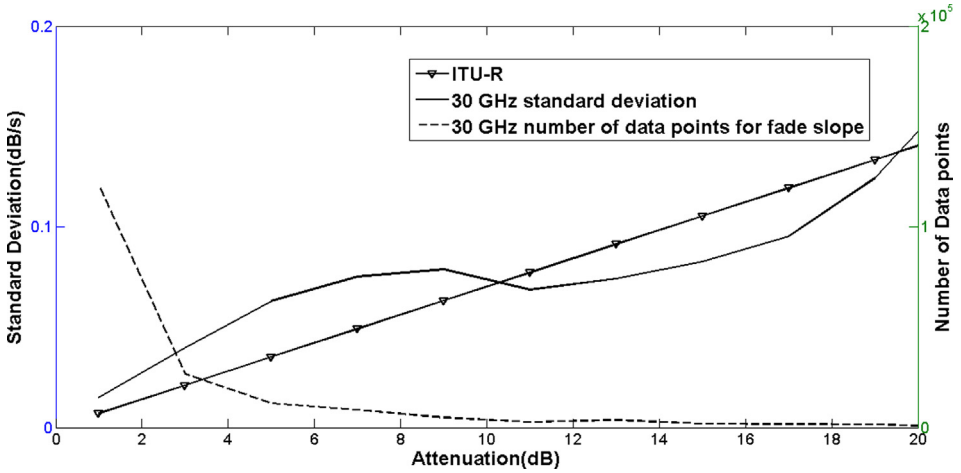

Fig. 6. Fade slope standard deviation as a function of attenuation, at 30 GHz for 2014 (solid line), compared to the ITU-R model predictions (solid line with triangle) and number of data points considered for calculation of fade slope (dashed line) for 30 GHz.

the considered data points are limited. That may be the reason behind much discrepancy between measured and modeled standard deviation of fade slope at 30 GHz.

3.3. Dependence of standard deviation with filter characteristics

Standard deviation is treated as the only controlling factor of the fade slope distribution in ITU-R model. Since standard deviation is dependent on filter cutoff frequency and sampling interval, therefore the equation for $F(f_b, \Delta t)$ is a function of time interval (Δt) (here it is considered as 2 sec) and the cut-off frequency of the low pass filter (f_b). This can be written as

$$\mathrm{F}(f_b, \Delta \mathrm{t}) = \sqrt{2\Pi^2/((1/{f_B}^b + (2\Delta \mathrm{t})^b)^{1/b})} \quad (2)$$

The value of b is taken as 2.3 (ITU-R P.1623 –1, 2005). The standard deviation can therefore be written as (ITU-R P.1623 –1, 2005)

$$\sigma_s = sF(f_b, \Delta t)A \quad (3)$$

The value of s is obtained from the experimental data and is shown in Fig. 7. A weighted mean of the fade slope standard deviation for the two frequencies at all attenuation thresholds are calculated and zero offset best fit of the weighted mean is estimated. The value of s is found to be 0.011 for Ahmedabad at an elevation angle of 63° that is similar to the ITU-R model (ITU-R P.1623 –1, 2005) derived value of 0.01. It is again noted here that the value of s at 30 GHz significantly varies from the best fit curve. However, it should be noted that the s parameter is very sensitive to amount of data and this is just a preliminary estimation. A comprehensive study of tropical region is required to conclude on the behavior of s.

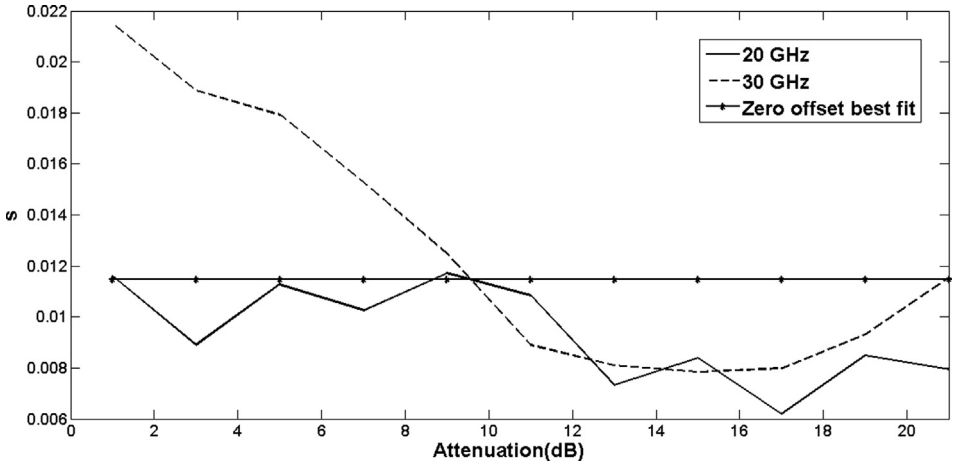

Fig. 7. Parameter s as a function of attenuation for both frequencies and the zero-offset best fit.

4. Conclusions

Fade slope characteristics at 20 GHz and 30 GHz are studied for Ahmedabad, a tropical location, with experimental measurements using GSAT-14 satellite. Over all, the ITU-R model does not match very well with measurements beyond a certain attenuation threshold level at 20 GHz and the deviation increases at 30 GHz. The s parameter is also found to be similar but does not exactly match the ITU-R model. It is to be noted, though ITU-R model is said to be applicable to link elevation only between 10°–50°, we observe a close match with experimental results at 63° as well. We also have observed a frequency dependence of the fade slope characteristics unlike the ITU-R model and it may be due to cloud attenuation at high frequencies. This trend may also be due to statistical instability of limited data set and needs further investigation.

Acknowledgment

Authors thankfully acknowledge the scientists of Space Applications Center, ISRO for providing the experimental data. Financial support received under DST- INSPIRE Faculty scheme and ISRO- RESPOND program are also thankfully acknowledged.

References

Adhikari, A., Das, S., Bhattacharya, A., Maitra, A., 2011. Improving rain attenuation estimation: modelling of effective path length using Ku-Band measurements at a tropical location. Prog. Electromag. Res. B 34, 173–186. https://doi.org/10.2528/PIERB11072503.

Amaya, C., Nguyen, T., 2010. Propagation measurements in Ottawa with the Ka-Band Beacon of the Anik F2Satellite. In: Proceedings of 14th International Symposium on Antennas and Electromagnetics (ANTEM), Ottawa, July 2010. https://doi.org/10.1109/ANTEM.2010.5552527.

Castanet, L., Bolea-Alamanac, A., Bousquet, M., 2003. Interference and fade mitigation techniques for Ka and Q/V band satellite communication systems. In: Proceedings of COST 272-280 International Workshop on Satellite Communications from Fade Mitigation to Service Provision, The Netherlands.

Cheffena, M., Amaya, C., 2008. Prediction model of fade duration statistics for Satellite Links between 10–50 GHz. IEEE Antennas Wirel. Propag. Lett. 7, 260–263. https://doi.org/10.1109/LAWP.2008.92 1369.

Chambers, A.P., Callaghan, S.A., Otung, I.E., 2006. Analysis of rain fade slope for Ka and V-Band satellite links in Southern England. IEEE Trans Antennas Propagat 54 (5), 1380–1387. https://doi.org/10.1109/TAP.2006.874318.

Das, S., Maitra, A., Shukla, A.K., 2010. Rain attenuation modeling in the 10–100 GHz frequency using drop size distributions for different climatic zones in tropical India. Prog. Electromag. Res. B 25, 211–224. https://doi.org/10.2528/PIERB10072707.

Das, S., Chakraborty, S., Maitra, A., 2013. Radiometric measurements of cloud attenuation at a tropical location in India. J. Atmos. Sol. Terr. Phys. 105–106, 97–100. https://doi.org/10.1016/j.jastp.2013.09.003.

Das, D., Maitra, A., 2016. Fade-Slope model for rain attenuation prediction in tropical region. IEEE Geosci. Remote Sens. Lett. 13, 777–781. https://doi.org/10.1109/LGRS.2016.2543299.

Das, S., Maitra, A., 2017. Characterization of tropical precipitation using drop size distribution and rain rate-radar reflectivity relation. Theor. Appl. Climatol. 132 (3), 275–286. https://doi.org/10.1007/s00704-017-2073-1.

Dao, H., Islam, R., Khateeb, K., 2013. Rain fade slope model in satellite path based on data measured in heavy rain zone. IEEE Antennas Wirel. Propag. Lett. 12, 50–53. https://doi.org/10.1109/LAWP.2012.2237 373.

Dao, H., Farez, M.A.Z., Islam, M.R., 2018. Rain fade duration prediction models for a high elevation angle based on measured data in tropical climate. Adv. Space Res. 62 (7), 1879–1883. https://doi.org/10.1016/j.asr.2018.06.032.

Debnath, A., Das, R.K., Gogoi, D., 2017. A study of Ka-band signal attenuation at Umiam, Meghalaya with ISRO's GSAT-14 satellite. ADBU-J. Eng. Technol. 6 (2), 00602610–00602614.

Green, H.E., 2004. Propagation impairment on Ka-band SATCOM links in tropical and equatorial regions. IEEE Antennas Propag. Mag. 46 (2), 31–45. https://doi.org/10.1109/MAP.2004.1305532.

ITU-R-R Recommendation P.1623–1, 2005. Prediction method of fade dynamics on Earth-space paths.

ITU-R-R Recommendation P.838–3, 2005. Specific attenuation model for rain for use in prediction methods.

ITU-R-R Recommendation P.618-13, 2017. Propagation data and prediction methods required for the design of Earth-space telecommunication systems.

Jong, S.L., Riva, C., Din, J., D'Amico, M., Lam, H.Y., 2019. Fade slope analysis for Ku-band earth-space communication links in Malaysia. IET Microwaves Antennas Propag. 13 (13), 2330–2335. https://doi.org/10.1049/iet-map.2018.6023.

Kamp, M.V., 2003. Statistical analysis of rain fade slope. IEEE Trans. Antennas Propag. 51 (8), 1750–1759. https://doi.org/10.1109/TAP.2003.808542.

Miranda, E.C.D., Pontes, M.S., Da Silva Mello, L.A.R., 1999. Fade slope statistics for three 12-GHz satellite beacon links in Brazil. IEEE Commun. Lett. 3 (5), 142–144. https://doi.org/10.1109/4234.766849.

Matricciani, E., Riva, C., 2008. 18.7 GHz tropospheric scintillation and simultaneous rain attenuation measured at Spino d'Adda and Darmstadt with Italsat. Radio Sci. 43 (01), 1–13. https://doi.org/10.1029/2007RS003688.

Ong, J.T., Zhu, C.N., Lee, Y.K., 1997. Ku-band satellite beacon attenuation and rain rate measurements in Singapore comparison with ITU-R models. In: Proceedings of 10th International Conference on Antennas and Propagation, IET. 2, 2153–2156. https://doi.org/10.1049/cp:19970352.

Pontes, M.S., Mirinda, E.C.D., Da Silva Mello, L.A.R., De Souza, R.S.L., De Almeida, M.P.C., 2003. Rainfall-induced satellite beacon attenuation in tropical and equatorial regions. Electron. Lett. 39 (11), 874–876. https://doi.org/10.1049/el:20030563.

Sarkar, T., Das, S., Maitra, A., 2014. Effects of melting layer on Ku-band signal depolarization. J. Atmos. Sol. Terr. Phys. 117, 95–100. https://doi.org/10.1016/j.jastp.2014.06.006.

Sujimol, M.R., Acharya, R., Sing, G., Gupta, R.K., 2015. Rain attenuation using Ka and Ku band beacons at Delhi earth station. Indian J Radio Space Phys. 44, 45–50.

Ventouras, S., Wrench, C.L., Callaghan, S.A., 2001. New thinking required to offset limitations imposed by V-band propagation. In: Proceedings of 19th AIAA Int. Comm. Sat. Sys. Conf, France.

Xin, Z., Zhenwei, Z., Leke, L., Changsheng, L., 2012. Rain fade slope on 12.5 GHz Earth-space link at Qingdao. In: Proceedings of 2012 International Conference on Microwave and Millimeter Wave Technology (ICMMT), IEEE. 4. https://doi.org/10.1109/ICMMT.2012.6230266.